3DPCT: 3D Point Cloud Transformer with Dual Self-attention

Dening Lu, Kyle (Yilin) Gao, *Graduate Student Member, IEEE,* Qian Xie, Linlin Xu, *Member, IEEE,* Jonathan Li, *Senior Member, IEEE*

Abstract—**Transformers have resulted in remarkable achievements in the field of image processing. Inspired by this great success, the application of Transformers to 3D point cloud processing has drawn more and more attention. This paper presents a novel point cloud representational learning network, 3D Point Cloud Transformer with Dual Self-attention (3DPCT) and an encoder-decoder structure. Specifically, 3DPCT has a hierarchical encoder, which contains two local-global dual-attention modules for the classification task (three modules for the segmentation task), with each module consisting of a Local Feature Aggregation (LFA) block and a Global Feature Learning (GFL) block. The GFL block is dual self-attention, with both point-wise and channel-wise self-attention to improve feature extraction. Moreover, in LFA, to better leverage the local information extracted, a novel point-wise self-attention model, named as Point-Patch Self-Attention (PPSA), is designed. The performance is evaluated on both classification and segmentation datasets, containing both synthetic and real-world data. Extensive experiments demonstrate that the proposed method achieved state-of-the-art results on both classification and segmentation tasks. *Our code will be made publicly available*.**

Index Terms—**Transformer, Graph convolution, Point cloud classification, Point cloud segmentation, Deep learning, Self-attention mechanism.**

I. INTRODUCTION

POINT cloud processing is a fundamental task in 3D computer vision. Point clouds, being flexible, simple, and with easy-to-use data structures, are commonly used in 3D mapping, robotics, autonomous navigation, and virtual reality. With the ever-increasing availability and affordability of 3D sensors in the form of LiDAR scanners and RGB-D cameras, low and high-level point cloud tasks and research thereof are ever more important. For these tasks, many types of deep learning architectures were experimented with in the recent past. Among these, the Transformer [1] architecture emerged as a powerful point cloud feature extraction backbone, performing exceedingly well on point cloud classification, detection, and segmentation [2]. First developed for natural language processing, the Transformer is a low-inductive bias network which is capable of learning both long-range and local features, depending on implementation. Since then, Transformers have successfully been applied to 2D and

(*Corresponding authors: Linlin Xu; Jonathan Li.*)

Dening Lu, Kyle Gao, Linlin Xu, and Jonathan Li are with the Department of Systems Design Engineering, University of Waterloo, Waterloo, Ontraio N2L 3G1, Canada (e-mail: d62lu, y56gao, l44xu, junli@uwaterloo.ca).

Jonathan Li is also with the Departmemt of Geography and Environmental Management, University of Waterloo, Waterloo, Ontario N2L 3G1, Canada.

Qian Xie is with the Department of Computer Science, University of Oxford, Oxford OX1 3QD, U.K. (e-mail: qian.xie@cs.ox.ac.uk).

3D computer vision in a wide variety of tasks, achieving state-of-the-art results across a wide variety of benchmarks.

The Transformer's representational power comes from the attention mechanism. Specific to point cloud applications, many recent works (Sec. II) explored both point-wise attention suited for learning spatial features, and channel-wise attention suited for feature refinement. By combining multi-scale k Nearest Neighbour (kNN) based Graph Convolution with the dual-type Transformer architecture with both point-wise and channel-wise attention, we proposed the 3DPCT, a powerful point hierarchical cloud transformer processing network with both classification and segmentation variants. Our 3DPCT achieved competitive results in part segmentation, and significantly exceeded previous best performing methods in both classification and semantic segmentation across popular benchmark datasets.

In summary, the main contributions of our work are as follows:

- To improve feature learning in Transformer, a novel global-local dual transformer approach was designed, where the global module contains both point-wise and channel-wise self-attention mechanisms. The point-wise mechanism was further improved with a novel point-wise self-attention approach, named PPSA, to mitigate the local information loss;
- A hierarchical encoder-decoder network, named 3DPCT, was constructed to integrate the global and local modules mentioned-above, leading to a general backbone for point cloud representation and analysis. The proposed framework is used for improving both 3D point cloud classification and segmentation.
- Extensive experiments on ModelNet40, ShapeNet, and Toronto3D showed that our method exceeded previous state-of-the-art performance in both classification and segmentation.

II. RELATED WORK

A. Transformers in 3D Point Cloud Processing

Transformers have achieved great success in the field of 3D point cloud processing. They have been applied to many common 3D tasks so far, such as classification, segmentation, and detection. Since our paper focused on applying the Transformer to point cloud classification and segmentation, we conducted a detailed survey to the related works on these two tasks, and presented an introduction to the theory of point cloud Transformers.
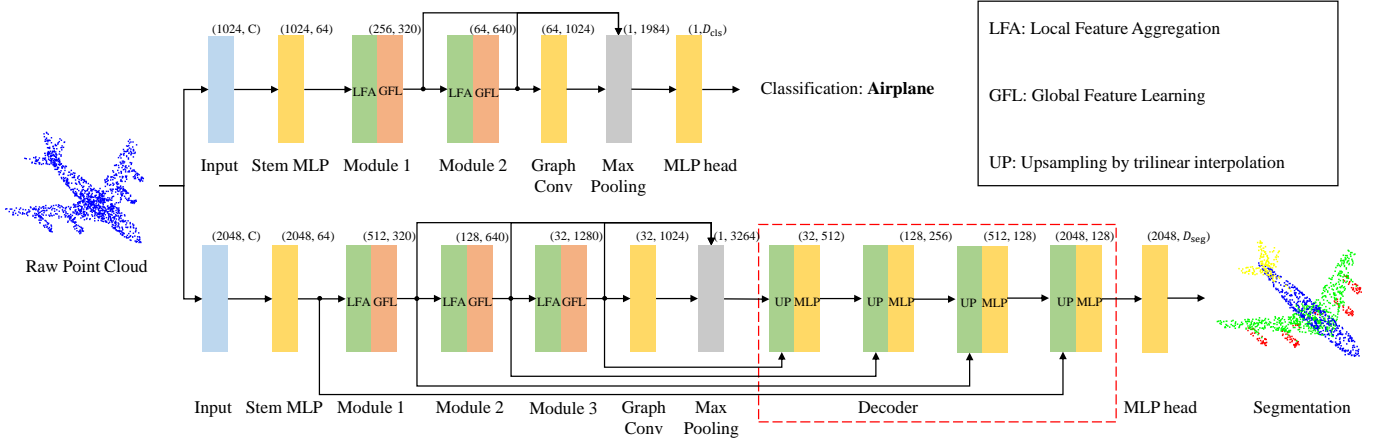
Fig. 1. 3DPCT networks for point cloud classification (top) and segmentation (bottom), where Graph Convolution-based LFA blocks and dual self-attention-based GFL blocks were designed for strong feature representation.

3D Point Cloud Classification. There exist a number of Transformer-based point cloud classification methods, which can be divided into two categories: point-wise Transformer methods and channel-wise Transformer methods. Specifically, the former uses the self-attention mechanism to capture long-and/or short-range dependencies among input points. Therefore, they can be further divided into global Transformer-based methods and local Transformer-based methods. However, for a channel-wise Transformer, instead of operating in the point space, it uses the self-attention mechanism to establish the relationship among different channels in the feature space.

Point Cloud Transformer (PCT), as a standard global Transformer network, was proposed in [3]. In PCT, all input points were leveraged for global feature extraction. PCT first adopted a neighborhood-embedding strategy to aggregate the local information, followed by feeding the embedded features into four stacked global Transformer blocks. Lastly, it utilized a global Max and Average (MA) pooling to extract the global information for point cloud classification. 3CROSSNet proposed in [4] used multi-scale global information for classification. Taking the raw point cloud as input, it first generated three point subsets with different resolutions by Farthest Point Sampling (FPS). Secondly, it established kNN neighborhoods and extracted local information by a series of Multi-Layer Perception (MLP) modules for each point subset. Thirdly, the cascaded global Transformer blocks were applied to extract the global information of each subset. Lastly, given the multi-scale global features, 3CROSSNet used the Cross-Level Cross-Attention (CLCA) and Cross-Scale Cross-Attention (CSCA) modules to capture long-range inter- and intra-level dependencies for classification. As a local Transformer network, Point Transformer (PT) [5] focused on extracting local information by the Transformer. It had five local Transformer blocks operated on the downsampling point sets. Specifically, for each block, it constructed kNN neighborhoods for sampling points, followed by utilizing a vector-attention mechanism to capture local features. After five local Transformer blocks, PT used a global MA pooling to extract the global feature for classification. Local Feature Transformer Network (LFT-Net) had a similar architecture. However, it used an additional trans-pooling module to alleviate the feature loss during the pooling.

The channel-wise Transformer has been proven to be effective in Geometric Back-projection Network (GBNet) [6]. GBNet used a Channel-wise Affinity Attention (CAA) module to capture the channel-wise global information. It had achieved state-of-the-art performance in point cloud classification. Dual Transformer Network (DTNet) [7] combined both the point-wise and channel-wise self-attention mechanisms for global feature extraction. The ablation experiments in DTNet showed that the combined global feature works better than any feature from only point-wise or only channel-wise self-attention mechanism. Inspired by DTNet, our paper also adopted a dual self-attention mechanism, i.e., both point-wise and channel-wise self-attention for global feature learning.

3D Point Cloud Segmentation. There are many Transformer-based segmentation networks that are developed from the corresponding classification networks. The segmentation network of PCT [3] took its classification network variant as the encoder. The decoder first concatenated the pooled global feature with each point feature, enhancing the perception of global information for each point. Then the concatenated features were fed into a series of MLP layers for dense prediction, following PointNet [8]. Similarly, PT [5] also developed the segmentation network based on its classification framework. The authors designed a U-net architecture for segmentation, where the decoder was symmetric to the encoder. Since it used a hierarchical structure in the encoder, a transition-up module with trilinear interpolation was proposed in the decoder for point cloud upsampling. Instead of using raw point clouds, Stratified Transformer [9] took 3D voxels as input to the segmentation network. It applied Transformers in predefined local windows, following Swin Transformer [10]. To capture the global information and establish connections between different windows, it presented a novel key sampling strategy, enlarging the effective receptive field for each $query$ point.

Despite the great success of Transformers in point cloud classification and segmentation, its massive linear operations tend to result in high computational footprint and memory consumption. Therefore, instead of Transformers, our paper was proposed to utilize the Graph Convolution method to achieve local information extraction, verifying the feasibility of combining Graph Convolution and Transformers. This operation contributes to the lightweight design of the Transformer network. Moreover, to alleviate the local information loss caused by pooling operations, we proposed a novel point-wise self-attention mechanism (PPSA), please refer to Sec. III-C for more details.

B. 3D Self-attention Mechanism

Corresponding to the point-wise and channel-wise Transformers, the self-attention mechanisms can likewise be divided into point-wise and channel-wise self-attention. With the development of 3D Transformers, there have been a number of self-attention variants designed to improve algorithm performance.

Point-wise Self-attention. The point-wise self-attention is the most commonly used mechanism in 3D Transformers. Point Attention (P-A) [11] and Attentional ShapeContextNet (A-SCN) [12] were the early works using the standard point-wise self-attention for point cloud processing and analysis. Recent 3D Transformer works have made a series of improvements. PCT [3] presented an Offset-Attention based on the Laplacian matrix in Graph Convolution Networks (GCNs) [13]. It also introduced a novel normalization method for the attention map, replacing $Scale + Softmax$ (SS) with $Softmax + L_1 Norm$ (SL). This operation was able to sharpen the attention weights and reduce the influence of noise. PT [5] introduced the vector attention to the point-wise self-attention mechanism. Such an attention mechanism made a more detailed assessment of the similarities among different feature points, resulting in stronger feature expression. Since the high computational cost is the key drawback of 3D Transformers, Centroid Transformer [14] was proposed to improve algorithm efficiency by reducing $Query$ points in the self-attention module. Specifically, it first used an optimized "soft K-means" to create M center points from N input points, followed by generating $Query$ and Key matrices based on M center points and N input points, respectively. As such, the computational cost of the self-attention was reduced to $O(NM)$ from $O(N^2)$. Light-weight Transformer Network (LighTN) [15] used a different way to reduce the computational cost of the self-attention module. It removed the weight matrices W_Q, W_K, and W_V, reducing trainable parameters for high efficiency. The authors named this self-attention variant the self-correlation mechanism, which achieved a satisfactory trade-off between the accuracy and efficiency of the algorithm.

Channel-wise Self-attention. The channel-wise self-attention mechanism has drawn more and more attention in the field of point cloud processing. DTNet [7] utilized the standard channel-wise self-attention for global feature extraction. GBNet [6] made further improvements to the aforementioned model, proposing a Channel-wise Affinity Attention (CAA) module. Specifically, GBNet authors designed a Compact Channel-wise Comparator (CCC) block to generate the attention map, measuring the similarities of different channels. Then they designed a Channel Affinity Estimator (CAE) block to generate an affinity matrix, avoiding similar/redundant information when generating attention features. This block was able to enhance global feature expression. Inspired by DTNet [7] and GBNet [6], we proposed a dual self-attention mechanism for global feature learning. Specifically, we designed a more effective point-wise self-attention, PPSA, and adopted the CAA-like channel-wise self-attention.

III. 3D CONVOLUTION-TRANSFORMER NETWORK

In this section, we introduced the encoder-decoder structure of our 3DPCT for both point cloud classification and segmentation. We first showed the pipeline of our method, then introduced the main modules in the encoder and decoder stages respectively.

A. Overview

Fig. 1 shows the overall pipeline of our method. We proposed a general backbone network for point cloud classification and segmentation. Our classification and segmentation networks both shared the same encoder architecture. After that, the classification network utilized an MLP head to obtain the final classification results, while the segmentation network utilized a decoder with trilinear interpolation-based upsampling for dense prediction, following PointNet++ [16].

The original point cloud with/without normal was taken as input to the encoder. We first designed a stem MLP block [17] to project the input data into a higher-dimension space. After that, the projected features were fed into several modules in a hierarchical manner for local and global feature extraction. Each module consisted of two blocks: multi-scale LFA block achieved by the Graph Convolution [18], and GFL block achieved by the Transformer. This way of combining the Graph Convolution and Transformer for semantic feature learning has been proved to be effective by [19]. Following this, we used the max-pooling operation on the output feature maps of each aforementioned module, to obtain the global feature of each level (module). Then, we concatenated them for multi-level global feature generation. Given the extracted global feature, we leveraged an MLP head for the point cloud classification task, which consisted of two fully connected layers with batch normalization and RELU activation. For the segmentation task, the extracted global feature was then taken as input to the decoder. To improve efficiency, we fully adopted the decoder structure of Pointnet++ [16], instead of a symmetric one. In the upsampling block, the interpolated points were concatenated with the corresponding feature points from the encoder via skip connection. We note that the number of the modules in the encoder and decoder can vary according to the number of input points, which is similar to [5], [16]. In our experiments, we designed a two-module encoder for the classification task (1024 input points), but a three-module encoder and corresponding decoder for the segmentation task (2048 input points).
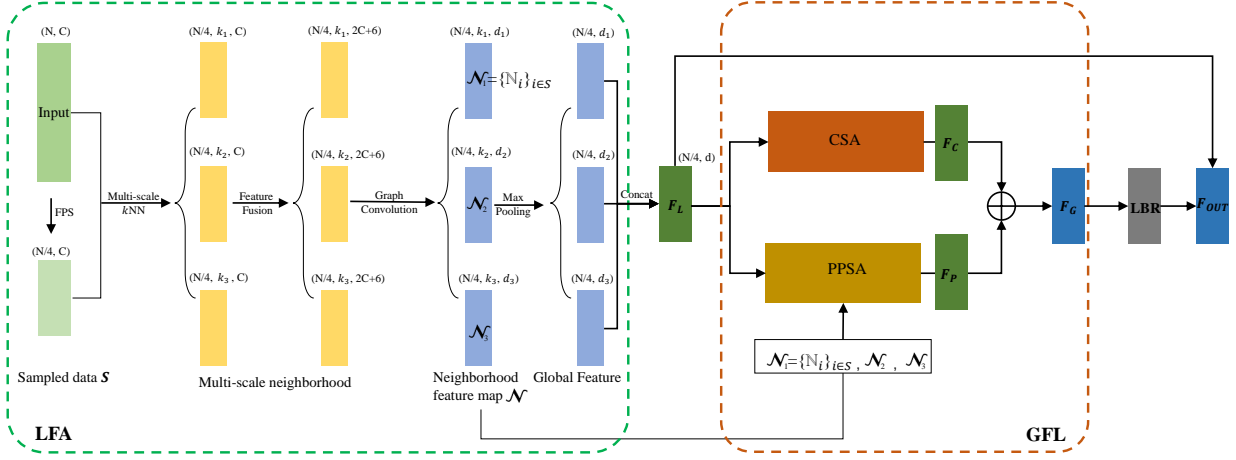
Fig. 2. Architecture of Module 1 structure, which consists of an LFA block and a GFL block.

B. Local Feature Aggregating Block

We adopted the Graph Convolution-based LFA block proposed in [19] for local feature aggregation. We introduced the LFA block (Fig. 2) as follows.

The input point cloud was first downsampled to $N/4$ points by FPS, generating a sampled point subset S, where N is the number of the input points. After that, the LFA block constructed multi-scale kNN neighborhoods (three scales k_1, k_2, k_3 in our experiments) for each sampled point, to ensure the diversity of the receptive fields. Furthermore, in each neighborhood χ_i of the sampled point S_i, a fused feature $\mathbb{C}_i$ of S_i was generated by combining its coordinate and feature information P_i, F_i:

$$\mathbb{C}_i = concat(F_i, P_i), \tag{1}$$

where F_i and P_i represent the semantic and geometric properties of S_i respectively. Given the fused neighborhood feature, the Graph Convolution in χ_i can be formulated as:

$$l_i = \underset{j \in \chi_i}{maxpooling} \left(Conv(\Delta\mathbb{C}_{ij}) \right), \tag{2}$$

where l_i is the aggregated local feature of S_i, $Conv$ is a convolution operation with 1×1 kernels, $\Delta\mathbb{C}_{ij}$ represents the relationship between the j-th neighborhood point χ_{ij} and S_i, which is defined as:

$$\Delta\mathbb{C}_{ij} = concat(F_{ij} - F_i, P_{ij} - P_i, \mathbb{C}_i), \tag{3}$$

where F_{ij} and P_{ij} represent the semantic and geometric properties of χ_{ij} respectively. Specifically, in Fig. 2, since the dimensions of the input feature map and corresponding point set are (N, C) and $(N, 3)$, the dimension of $\Delta\mathbb{C}_{ij}$ is $2C + 6$. Furthermore, we defined different output dimensions of Graph Convolution for different scale neighborhoods: d_1, d_2, and d_3, where $d_1 < d_2 < d_3$ ($k_1 < k_2 < k_3$). In [18], $\Delta\mathbb{C}_{ij}$ is also called the edge function. $Conv(\Delta\mathbb{C}_{ij})$ establishes semantic and geometric relationships between the sampling point S_i and neighborhood point χ_{ij}. As such, a neighborhood feature set containing local information, $\mathbb{N}_i$ of S_i, was generated. Then, the max-pooling operation was used to aggregate the local

information to S_i. Given the aggregated local feature l_i of S_i at each scale, we finally concatenated them to generate the multi-scale local feature L_i of S_i, which can be expressed as:

$$L_i = concat(l_{i1}, l_{i2}, l_{i3}), \tag{4}$$

where l_{i1}, l_{i2}, l_{i3} denote three local features of S_i at three different scales.

C. Global Feature Learning Block

Our GFL block contained two kinds of self-attention mechanisms: Point-wise Self-Attention (PSA), and Channel-wise Self-Attention (CSA). PSA was utilized to establish the spatial relationship among points and model long-range context dependencies, which has been commonly used in 3D Transformer methods [3], [19], [20]. Moreover, to leverage all the local information extracted from the LFA block, we presented a new point-wise self-attention mechanism, PPSA. CSA was utilized to measure the correlation among different feature channels. It was able to improve context information modeling by highlighting the role of interaction across various channels, which has been proven effective in [6], [7]. A detailed introduction to these two mechanisms is as follows.

Point-Patch Self-Attention (PPSA). In this subsection, we presented a new point-wise self-attention mechanism, PPSA, which was designed to not only utilize the sampling points but also leverage their neighborhood (patch) information for global feature learning. As shown in Fig. 3, the aggregated features $F_L = \{L_i\}_{i \in s} \in R^{s \times d}$ from the LFA block was taken as input, where s is the number of sampled points in S, and d denotes the feature dimension of F_L. We first projected F_L into two different feature spaces to generate $Query$, Key matrices:

$$\begin{aligned} Query &= F_L W_{QP}, \\ Key &= F_L W_{KP}, \end{aligned} \tag{5}$$

where W_{QP}, W_{KP} are learnable weight matrices. Then, the attention map $M_P \in R^{s \times s}$ of PPSA can be formulated as:

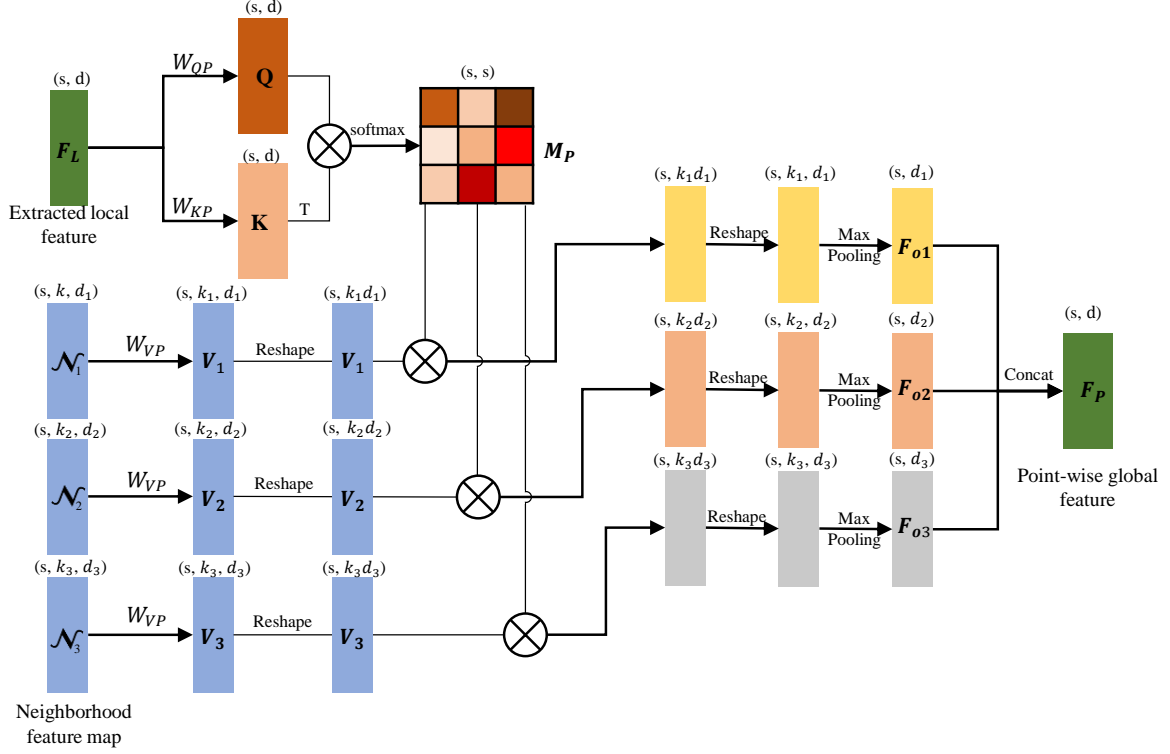$$M_P = softmax(\frac{QK^T}{\sqrt{d}} + B), \tag{6}$$

Fig. 3. Point-Patch Self-Attention mechanism. It utilized the sampling point features and the corresponding neighborhood (patch) feature maps for point-wise global feature extraction.

where Q, K denote the $Query$, Key matrices, and B is a learnable position encoding matrix defined by [5]. Inspired by [21], we directly treated the neighborhood feature map $\mathcal{N} = \{\mathbb{N}_i\}_{i \in s}$ at each scale as the $Value$ branch, instead of F_L. In other words, the elements in the attention map were taken as weights of the corresponding neighborhood feature sets $\mathbb{N}_i$. Then, the output neighborhood feature was obtained by computing a weighted sum of all input sets. As such, we were able to leverage all the points including sampling points and neighborhood points for the global information extraction, instead of only sampling points. This method can mitigate the local information loss caused by the pooling operation in Eq. 2. Given the aforementioned attention map M_P and the $Value$ matrix, the output global feature can be expressed as:

$$F_o = maxpooling\,(M_P V), \qquad (7)$$

where V denotes the $Value$ matrix, i.e., $\mathcal{N}$. The detailed algorithm flow and feature dimension transformation of PPSA are shown in Fig. 3. Lastly, we concatenated the F_o at each scale to get the final point-wise global feature F_P:

$$F_P = concat(F_{o1}, F_{o2}, F_{o3}), \qquad (8)$$

where F_{o1}, F_{o2}, F_{o3} were generated from neighborhood feature maps at different scales.

Channel-wise Self-Attention (CSA). Apart from the point-wise self-attention mechanism, we also utilized the channel-wise self-attention to capture context dependencies in the channel dimension, enhancing the feature expression of our model. As shown in Fig. 4, given the aggregated local feature $F_L \in R^{s \times d}$, we first computed the attention map $M_C \in R^{d \times d}$ of CSA as:

$$M_C = K^T Q = (F_L W_{KC})^T (F_L W_{QC}). \qquad (9)$$

where the shapes of K, Q were reduced to $(s/8) \times d$ by weight matrices W_{KC} and W_{QC}, to improve efficiency. Inspired by [6], we calculated the affinity matrix A_C based on M_C, to measure the difference among channels, which can be expressed as:

$$A_C = softmax(expand(maxpooling(M_C)) - M_C), \quad (10)$$

where $maxpooling(M_C) \in R^{d \times 1}$ extracts the maximum value of each row in M_C, $expand(\cdot)$ expands the matrix $maxpooling(M_C)$ to the same size as M_C by column repetition. From the subtraction, the larger in magnitude the element in A_C, the lower the similarity of the corresponding two channels. As such, CSA tends to focus on channels with significant differences, avoiding aggregating similar/redundant information. After that, we calculated the $Value$ matrix as:

$$V = F_L W_{VC}, \qquad (11)$$

where W_{VC} is a learnable weight matrix. Finally, the channel-wise global feature F_C can be expressed as:

$$F_C = V A_C. \qquad (12)$$

Given both point- and channel-wise global features, the final global feature can be generated by combining them with an element-wise addition:
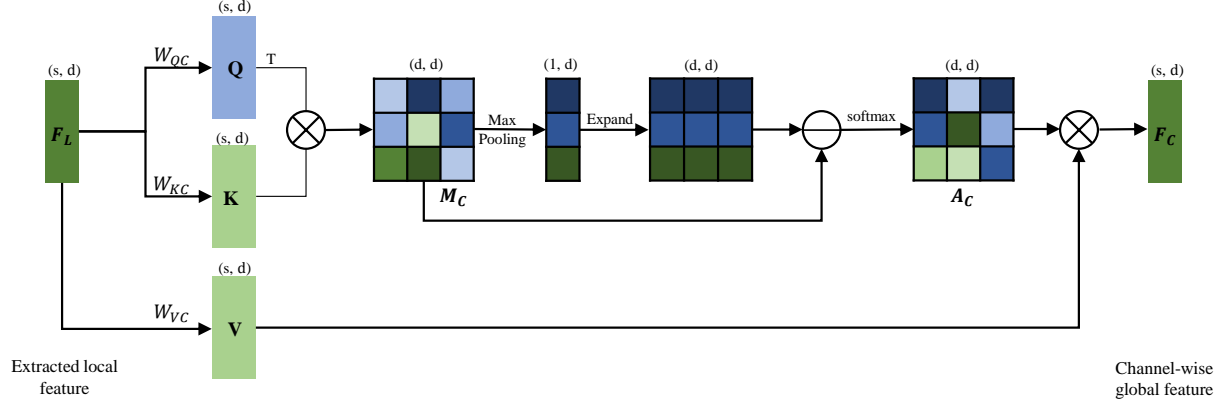
$$F_G = F_P + F_C. \qquad (13)$$

Fig. 4. Channel-wise self-attention mechanism. An Affinity matrix A_C was designed to avoid aggregating redundant features, enhancing the channel-wise global feature representation.

TABLE I
CLASSIFICATION RESULTS ON THE MODELNET40 DATASET

Methods	Input Size	mAcc (%)	OA (%)	Parameters (MB)	FLOPs (GB)	FPS
Other Learning-based Methods						
3DShapeNets [22]	1024	77.3	84.7	-	-	-
PointNet [8]	1024	86.0	89.2	3.47	0.45	**614**
PointNet++ [16]	1024	88.2	91.9	1.74	4.09	16
diffConv [23]	1024	90.4	93.2	2.08	**0.16**	-
CurveNet [24]	1024	90.4	93.1	-	-	-
PointCNN [25]	1024	88.1	92.2	**0.6**	1.54	14
DGCNN [18]	1024	90.2	92.2	1.81	2.43	279
FatNet [26]	1024	90.6	93.2	-	-	-
DRNet [27]	1024	-	93.1	-	-	-
PointNeXt [17]	1024	91.1	94.0	4.5	6.5	-
PointMLP [28]	1024	91.4	**94.5**	12.6	-	112
Transformer-based Methods						
PATs [29]	1024	-	91.7	-	-	-
LFT-Net [30]	1024	89.7	93.2	-	-	-
PointTransformer [31]	1024	89.0	92.8	13.86	9.36	17
MLMST [32]	1024	-	92.9	-	-	-
PointCloudTransformer [3]	1024	90.3	93.2	**2.80**	**2.02**	**125**
LSLPCT [33]	1024	90.5	93.5	-	-	-
PointTransformer [5]	1024	90.6	93.7	9.14	17.14	15
CloudTransformers [34]	1024	90.8	93.1	22.91	12.69	12
GBNet [6]	1024	91.0	93.8	8.38	9.02	102
3DCTN [19]	1024	91.6	93.2	4.21	3.76	24
Ours	1024	**92.4**	**94.0**	5.21	3.09	15

Additionally, we applied a residual connection between the LFA block and GFL block:

$$F_{OUT} = F_L + LBR(F_G), \tag{14}$$

where F_{OUT} is the final output feature map of the defined Module, and LBR denotes the combination of $Linear$, $BatchNorm$, and $ReLU$ layers.

IV. EXPERIMENTS

In this section, we first introduced the implementation of our 3DPCT, including hardware configuration and hyperparameter settings. Secondly, we presented the performance evaluation of our method on the classification and segmentation tasks, comparing it to state-of-the-art methods. Specifically, for the classification task, we tested our method on the widely-used ModelNet40 dataset [22]. For the object part segmentation task, we tested our method on the ShapeNet dataset [35]. For the semantic segmentation, we tested our method on the challenging Toronto3D dataset [36]. Finally, we presented the ablation experiment results on the main components of our method.

A. Implementation

We implemented our classification and segmentation networks in Pytorch. Both of them were trained and tested on an NVIDIA Tesla V100 GPU. We used the SGD Optimizer with a momentum of 0.9 and weight decay of 0.0001. The initial learning rate was set to 0.01, with a cosine annealing schedule to adjust the learning rate for each epoch. We trained classification, part segmentation, and semantic segmentation networks for 250, 300, and 500 epochs respectively, with the same batch size of 16.

B. Classification on ModelNet40 Dataset

Dataset and Metric. The ModelNet40 dataset contains 12311 CAD models with 40 object categories. We split them

into 9843 training samples and 2468 testing models, following PoineNet++ [16]. For a fair comparison, we downsampled each input point cloud to 1024 points with normals by Farthest Point Sampling. Since point clouds in ModelNet40 are generated from 3D meshes, we can easily obtain the normal of each point according to the corresponding face normal. The mean accuracy within each category (mAcc) and the overall accuracy (OA) were used for performance evaluation. Additionally, we adopted the total number of parameters, FLOPs (FLOating Point operations), and FPS (Frame Per Second) to evaluate the model size and efficiency.

Performance Comparison. We compared our 3DPCT with the state-of-the-art Transformer-based methods and other deep learning-based methods. The comparison results are shown in Table. I. As can be seen, our method achieved the best mean accuracy of 92.4% among all benchmarked methods in terms of mAcc, outperforming the prior state-of-the-art (PointMLP) by 1.0 absolute percentage point. In terms of OA, our method achieved the best result of 94.0% among the Transformer-based methods. For the model size, our method required fewer parameters (5.21MB) and FLOPs (3.09GB) compared to most Transformer-based algorithms, accounting for only 57% and 18% of PointTransformer respectively. However, due to naive implementation of several time-consuming operations like downsampling and kNN neighborhood construction, the inference speed of our method can still be improved.

Heat Map Visualization. Fig. 5 shows heat map visualization results to verify the interpretability of our method. Specifically, we obtained the regions of interest of our network for several point clouds of the Airplane, Car, Cup, and Plant classes by the Grad-CAM method [37]. From the results, the attention (colored in red) is mainly focused on the wings and tail of the Airplane, the tires of the Car, the handle of the Cup, and the leaves of the Plant. As we can see, all the regions of interest are consistent with the human visual system, demonstrating our method's interpretability.

TABLE II
PART SEGMENTATION RESULTS ON THE SHAPENET DATASET

Methods	Cat. mIoU	Ins. mIoU
PointNet [8]	80.4	83.7
A-SCN [12]	-	84.6
PointNet++ [16]	81.9	85.1
PCNN [38]	81.8	85.1
SpiderCNN [39]	82.4	85.3
SPLATNet [40]	83.7	85.4
Point2Sequence [41]	-	85.2
DGCNN [18]	82.3	85.2
SGPN [42]	82.8	85.8
SubSparseCNN [43]	83.3	86.0
PointCNN [25]	84.6	86.1
PointConv [44]	82.8	85.7
PVCNN [45]	-	86.2
RS-CNN [46]	84.0	86.2
KPConv [47]	85.0	86.2
InterpCNN [48]	84.0	86.3
DensePoint [49]	84.2	86.4
PAConv [50]	84.6	86.1
PointTransformer [5]	83.7	**86.6**
StratifiedTransformer [9]	**85.1**	**86.6**
Ours	84.0	**86.6**

C. Part Segmentation on ShapeNet Dataset

Dataset and Metric. The ShapeNet dataset contains 16880 models with 16 shape categories. We split them into 14006 training samples and 2874 testing models, following Point-Transformer [5]. The dataset has 50 part labels, and each object has at least two parts. For a fair comparison, we down-sampled each input point cloud to 2048 points with normals by FPS. The category-wise mean Intersection over Union (mIoU) and instance-wise mIoU were used for performance evaluation.

Performance Comparison. The comparison results are shown in Table. II. As measured by instance-wise mIoU, Our 3DPCT achieved competitive results (86.6%) compared with the SOTA Transformer-based methods such as Stratified Transformer [9]. Several part segmentation results are shown in Fig. 6.

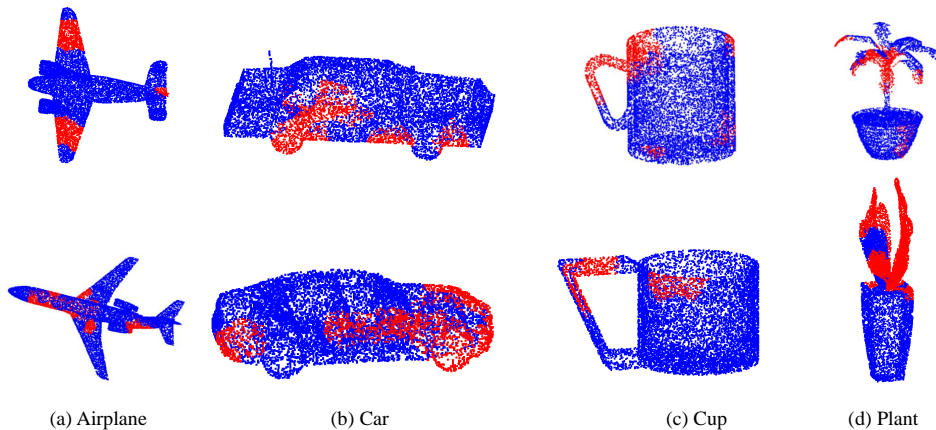| (a) Airplane | (b) Car | (c) Cup | (d) Plant |

Fig. 5. Heat map visualization of classification results. As can be seen, the attention (red) is focused on the discriminative parts of targets, such as the wings of an airplane, the tires of a car, the handle of a cup, and the leaves of a plant.

TABLE III
SEMANTIC SEGMENTATION RESULTS ON THE TORONTO3D DATASET

Methods	mIoU	Road	Road mrk.	Natural	Building	Util.line	Pole	Car	Fence
PointNet++ [16]	56.55	91.44	7.59	89.80	74.00	68.60	59.53	52.97	7.54
PointNet++ (MSG) [8]	53.12	90.67	0.00	86.68	75.78	56.20	60.89	44.51	10.19
DGCNN [18]	49.60	90.63	0.44	81.25	63.95	47.05	56.86	49.26	7.32
KPFCNN [47]	60.30	90.20	0.00	86.79	**86.83**	81.08	73.06	42.85	21.57
MS-PCNN [51]	58.01	91.22	3.50	90.48	77.30	62.30	68.54	52.63	17.12
TG-Net [52]	58.34	91.39	10.62	91.02	76.93	68.27	66.25	54.10	8.16
MS-TGNet [36]	60.96	90.89	18.78	**92.18**	80.62	69.36	71.22	51.05	13.59
PointCloudTransformer [3]	79.32	79.77	59.51	75.78	84.29	77.78	82.00	79.51	95.92
diffConv [23]	76.73	**83.31**	51.06	69.04	79.55	80.48	84.41	76.19	89.83
Ours	**82.53**	83.18	**59.51**	84.70	86.03	**83.98**	**85.19**	**81.14**	**96.17**

D. Semantic Segmentation on Toronto3D Dataset

Dataset and Metric. Toronto3D is a challenging real-scene dataset, collected by a 32-line LiDAR sensor in large-scale urban outdoor scenarios. It covers approximately 1 km of road and consists of about 78.3 million points, labeled into 8 different categories. The dataset has been divided into four subsets: $L001$, $L002$, $L003$, and $L004$, where $L002$ was taken as the testing set, and the others were taken as the training set. We further divided each subset into $5m \times 5m$ blocks and sampled 2048 points in each block, following diffConv [23]. The category-wise mIoU was used for performance evaluation. Additionally, the IoU for each category was also provided.

Performance Comparison. The comparison results are shown in Table. III. As can be seen, our 3DPCT outperformed all benchmarked methods in terms of category-wise mIoU. It surpassed the prior SOTA methods such as diffConv by 5.7 absolute percentage points. The Table also shows the specific IoU of each category, where our method achieved the best results in five of the eight categories, even for small objects like road marks. The results demonstrate that our method has excellent performance when processing real-scanned data, exceeding previous SOTA.

E. Ablation Study

We conducted a series of ablation experiments for the main components of our 3DPCT to verify their effectiveness. These experiments were performed on the ModelNet40 dataset.

Local Feature Aggregating Block. We first investigated the effectiveness of the LFA block, which was used to capture local information. As shown in Table. IV Row 2, the performance with the MLP-based LFA block was 91.6%/93.1% in terms of mAcc/OA, which was lower than that with the standard LFA block (92.4%/94.0%). This demonstrates that the Graph Convolution-based LFA block plays an important role in our algorithm. We also replaced the multi-scale strategy of the LFA block with the single-scale one. From the result in Table. IV Row 3, the classification performance of the multi-scale strategy was better than the single-scale strategy (91.3%/92.9%). This suggests that the multi-scale features are beneficial to enhancing the expression of local information, thereby improving the performance of our algorithm.

Global Feature Learning Block. We conducted a detailed ablation study on the GFL block. As shown in Table. IV, firstly, we removed the GFL block. As can be seen, the performance dropped significantly, which demonstrates that the GFL block is essential to our algorithm. Secondly, since the GFL block contained two important mechanisms: point-wise self-attention and channel-wise self-attention, we also studied the effectiveness of each mechanism. When the channel-wise self-attention was removed, the classification accuracy (mAcc/OA) dropped from 92.4%/94.0% to 91.9%/93.7%. Likewise, when the point-wise self-attention (PPSA) was removed, there was a similar drop (from 92.4%/94.0% to 91.13%/93.2%). These results suggest that both self-attention mechanisms are effective in improving classification performance. Additionally, to

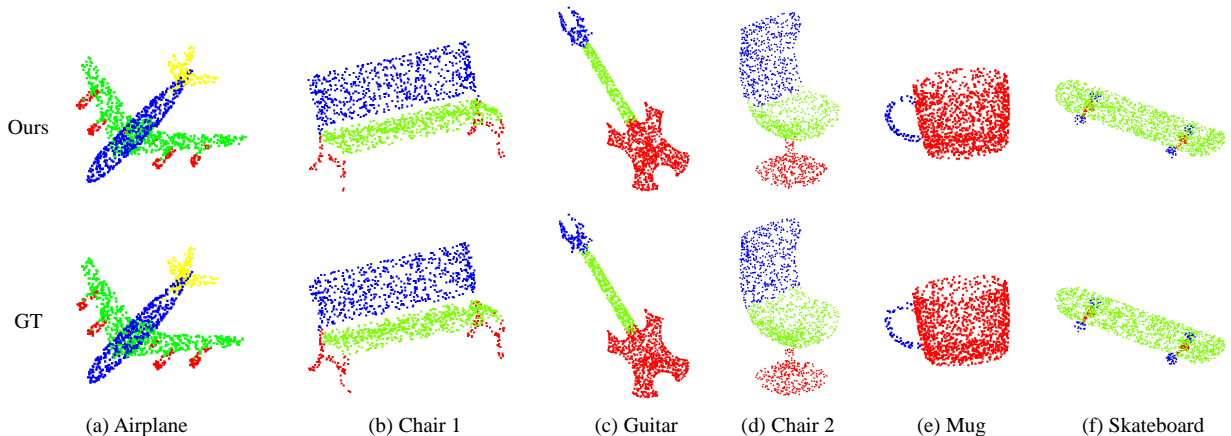|					
(a) Airplane	(b) Chair 1	(c) Guitar	(d) Chair 2	(e) Mug	(f) Skateboard

Fig. 6. Part segmentation results from the ShapeNet dataset. As can be seen, our segmentation predictions are faithful to the ground truth.

TABLE IV
ABLATION STUDY

Ablation		mAcc (%)	OA (%)	Parameters (MB)	FLOPs (GB)	FPS
Local feature aggregating	Graph convolution → Standard MLP	91.6	93.1	5.18	0.45	17
	Multi-scale → Single-scale	91.3	92.9	2.11	0.64	19
Global feature learning	−	91.2	92.7	2.25	2.78	17
	− CSA	91.9	93.7	4.71	3.04	16
	− PPSA	91.3	93.2	3.75	2.95	16
	PPSA → Standard PSA	91.5	93.6	5.11	3.08	15
Multi-level global feature	−	92.1	93.6	4.75	3.09	15
3DPCT		**92.4**	**94.0**	5.21	3.09	15

further verify the superiority of the PPSA mechanism, we replaced it with a regular point-wise self-attention mechanism (treating the F_L as the $Value$ matrix). After replacing, we observed a 0.9% and 0.4% drop in mAcc and OA respectively. This confirms the superiority of our PPSA mechanism.

Multi-level Global Feature Concatenation. We studied the effectiveness of the multi-level global feature. As illustrated in Fig. 1, we concatenated the output global feature of each level (module) by a residual connection to generate the multi-level global feature. As shown in Table. IV Row 8, when the residual connection was removed, we observed a 0.3% and 0.4% drop in mAcc and OA respectively. This suggests that the multi-level global feature contributes significantly to performance improvement.

V. CONCLUSION

In this paper, we have proposed a hierarchical point cloud representation network for classification and segmentation, named 3DPCT, composed of an encoder and a classification head/decoder. Taking the point cloud, either with or without normals as input, the encoder first projected it into a higher-dimensional space by using stem MLP, followed by feeding the projected feature map into several cascaded modules for local and global feature extraction. Specifically, each module consisted of a Graph Convolution-based LFA block and a Transformer-based GFL block. We designed a novel dual self-attention mechanism in the GFL block to improve the feature expression, which combined both point-wise and channel-wise self-attention features. Additionally, instead of the standard point-wise self-attention, we developed the PPSA mechanism to leverage local features of all input points, mitigating the local information loss. Then, the extracted features from the aforementioned modules were concatenated, followed by being fed into an additional Graph Convolution layer and further a max-pooling layer to generate the final global feature for classification. For segmentation, while taking the generated global feature as input, we adopted an All-MLP decoder following [16]. Extensive experiments on the Model-Net40 classification dataset [22], ShapeNet part segmentation dataset [35], and Toronto3D semantic segmentation dataset [36] demonstrated the superiority of our method in dealing with both synthetic and real-scene data.

Future Work. Our hierarchical network used Euclidean distance-based downsampling and neighborhood search, which are time-consuming and cannot serve the semantic information extracted by the network very well. Since the attention map in the Transformer contains rich feature relationships, we plan to utilize the attention map for semantic-based point cloud Sampling and Grouping as a future research project. To this end, the "superpoint" strategy could be a potential solution.

REFERENCES

[1] A. Vaswani *et al.*, "Attention is all you need," in *Proc. 31st Int. Conf. Neural Inf. Process. Syst.*, 2017, pp. 6000–6010.

[2] D. Lu, Q. Xie, M. Wei, L. Xu, and J. Li, "Transformers in 3d point clouds: A survey," *arXiv:2205.07417*, 2022. [Online]. Available: http://arxiv.org/abs/2205.07417

[3] M.-H. Guo, J.-X. Cai, Z.-N. Liu, T.-J. Mu, R. R. Martin, and S.-M. Hu, "PCT: Point cloud transformer," *Comput. Vis. Media.*, vol. 7, no. 2, pp. 187–199, Jun, 2021, doi:10.1007/s41095-021-0229-5.

[4] X.-F. Han, Z.-Y. He, J. Chen, and G.-Q. Xiao, "3CROSSNet: Cross-level cross-scale cross-attention network for point cloud representation," *IEEE Robotics Autom. Lett.*, vol. 7, no. 2, pp. 3718–3725, 2022.

[5] H. Zhao, L. Jiang, J. Jia, P. H. Torr, and V. Koltun, "Point transformer," in *Proc. IEEE Int. Conf. Comput. Vis.*, 2021, pp. 16 259–16 268.

[6] S. Qiu, S. Anwar, and N. Barnes, "Geometric back-projection network for point cloud classification," *IEEE Trans. Multimedia*, vol. 24, pp. 1943–1955, 2022.

[7] X.-F. Han, Y.-F. Jin, H.-X. Cheng, and G.-Q. Xiao, "Dual transformer for point cloud analysis," *arXiv:2104.13044*, 2021. [Online]. Available: http://arxiv.org/abs/2104.13044

[8] C. R. Qi, H. Su, K. Mo, and L. J. Guibas, "PointNet: Deep learning on point sets for 3D classification and segmentation," in *Proc. IEEE Conf. Comput. Vis. Pattern Recognit.*, 2017, pp. 77–85.

[9] X. Lai *et al.*, "Stratified transformer for 3D point cloud segmentation," in *Proc. IEEE Conf. Comput. Vis. Pattern Recognit.*, 2022, pp. 8500–8509.

[10] Z. Liu, Y. Lin, Y. Cao, H. Hu, Y. Wei, Z. Zhang, S. Lin, and B. Guo, "Swin transformer: Hierarchical vision transformer using shifted windows," in *Proc. IEEE Int. Conf. Comput. Vis. (ICCV)*, Oct. 2021, pp. 9992–10 002, doi:10.1109/ICCV48922.2021.00986.

[11] M. Feng, L. Zhang, X. Lin, S. Z. Gilani, and A. Mian, "Point attention network for semantic segmentation of 3D point clouds," *Pattern Recognit.*, vol. 107, p. 107446, 2020, doi:10.1016/j.patcog.2020.107446.

[12] S. Xie, S. Liu, Z. Chen, and Z. Tu, "Attentional shapecontextnet for point cloud recognition," in *Proc. IEEE Conf. Comput. Vis. Pattern Recognit.*, 2018, pp. 4606–4615.

[13] J. Bruna, W. Zaremba, A. Szlam, and Y. LeCun, "Spectral networks and locally connected networks on graphs," in *Proc. Int. Conf. Learn. Represent.*, 2014.

[14] L. Wu, X. Liu, and Q. Liu, "Centroid transformers: Learning to abstract with attention," *arXiv:2102.08606*, 2021. [Online]. Available: http://arxiv.org/abs/2102.08606

[15] X. Wang, Y. Jin, Y. Cen, T. Wang, B. Tang, and Y. Li, "LighTN: Light-weight transformer network for performance-overhead tradeoff in point cloud downsampling," *arXiv:2202.06263*, 2022. [Online]. Available: http://arxiv.org/abs/2202.06263

[16] C. R. Qi, L. Yi, H. Su, and L. J. Guibas, "PointNet++: Deep hierarchical feature learning on point sets in a metric space," in *Proc. 31st Int. Conf. Neural Inf. Process. Syst.*, 2017, p. 5105–5114.

[17] G. Qian *et al.*, "PointNeXt: Revisiting PointNet++ with improved training and scaling strategies," *arXiv:2206.04670*, 2022. [Online]. Available: http://arxiv.org/abs/2206.04670

[18] Y. Wang, Y. Sun, Z. Liu, S. E. Sarma, M. M. Bronstein, and J. M. Solomon, "Dynamic graph CNN for learning on point clouds," *ACM Trans. Graph.*, vol. 38, no. 5, pp. 1–12, 2019.

[19] D. Lu, Q. Xie, K. Gao, L. Xu, and J. Li, "3DCTN: 3D convolution-transformer network for point cloud classification," *IEEE Trans. Intell. Transport. Syst.*, 2022, doi:10.1109/TITS.2022.3198836.

[20] X. Yan, C. Zheng, Z. Li, S. Wang, and S. Cui, "PointASNL: Robust point clouds processing using nonlocal neural networks with adaptive sampling," in *Proc. IEEE Conf. Comput. Vis. Pattern Recognit.*, 2020, pp. 5589–5598.

[21] W. Li, X. Wang, X. Xia, J. Wu, X. Xiao, M. Zheng, and S. Wen, "Sepvit: Separable vision transformer," *arXiv:2203.15380*, 2022. [Online]. Available: http://arxiv.org/abs/2203.15380

[22] Z. Wu, S. Song, A. Khosla, F. Yu, L. Zhang, X. Tang, and J. Xiao, "3D shapenets: A deep representation for volumetric shapes," in *Proc. IEEE Conf. Comput. Vis. Pattern Recognit.*, 2015, pp. 1912–1920.

[23] M. Lin and A. Feragen, "diffconv: Analyzing irregular point clouds with an irregular view," *arXiv:2111.14658*, 2021. [Online]. Available: http://arxiv.org/abs/2111.14658

[24] A. Muzahid, W. Wan, F. Sohel, L. Wu, and L. Hou, "Curvenet: Curvature-based multitask learning deep networks for 3D object recognition," *IEEE CAA J. Autom. Sinica*, vol. 8, no. 6, pp. 1177–1187, 2021, doi:10.1109/JAS.2020.1003324.

[25] Y. Li, R. Bu, M. Sun, W. Wu, X. Di, and B. Chen, "PointCNN: Convolution on X-transformed points," in *Proc. Adv. Neural Inf. Process. Syst.*, vol. 31, 2018, pp. 820–830.

[26] C. Kaul, N. Pears, and S. Manandhar, "FatNet: A feature-attentive network for 3D point cloud processing," in *Proc. Int. Conf. on Pattern Recog. (ICPR)*, Jan. 2020, pp. 7211–7218, doi:10.1109/ICPR48806.2021.9412731.

[27] S. Qiu, S. Anwar, and N. Barnes, "Dense-resolution network for point cloud classification and segmentation," in *Proc. IEEE Winter Conf. Appl. Comput. Vis. (WACV)*, Jan. 2021, pp. 3813–3822, doi:10.1109/WACV48630.2021.00386.

[28] X. Ma, C. Qin, H. You, H. Ran, and Y. Fu, "Rethinking network design and local geometry in point cloud: A simple residual MLP framework," in *Proc. Int. Conf. Learn. Represent (ICLR)*, 2022.

[29] J. Yang, Q. Zhang, B. Ni, L. Li, J. Liu, M. Zhou, and Q. Tian, "Modeling point clouds with self-attention and gumbel subset sampling," in *Proc. IEEE Conf. Comput. Vis. Pattern Recognit. (CVPR)*, Jun. 2019, pp. 3323–3332, doi:10.1109/CVPR.2019.00344.

[30] Y. Gao, X. Liu, J. Li, Z. Fang, X. Jiang, and K. M. S. Huq, "Lft-net: Local feature transformer network for point clouds analysis," *IEEE Trans. Intell. Transport. Syst.*, 2022, doi:10.1109/TITS.2022.3140355.

[31] N. Engel, V. Belagiannis, and K. Dietmayer, "Point transformer," *IEEE Access.*, vol. 9, pp. 134 826–134 840, 2021, doi:10.1109/ACCESS.2021.3116304.

[32] X.-F. Han, Y.-J. Kuang, and G.-Q. Xiao, "Point cloud learning with transformer," *arXiv:2104.13636*, 2021. [Online]. Available: http://arxiv.org/abs/2104.13636

[33] Y. Song, F. He, Y. Duan, T. Si, and J. Bai, "Lslpct: An enhanced local semantic learning transformer for 3D point cloud analysis," *IEEE Trans. Geosci. Remote Sens.*, 2022, doi:10.1109/TGRS.2022.3202823.

[34] K. Mazur and V. Lempitsky, "Cloud transformers: A universal approach to point cloud processing tasks," in *Proc. IEEE Int. Conf. Comput. Vis. (ICCV)*, Oct. 2021, pp. 10 695–10 704, doi:10.1109/ICCV48922.2021.01054.

[35] L. Yi *et al.*, "A scalable active framework for region annotation in 3D shape collections," *ACM Trans. Graph.*, vol. 35, no. 6, pp. 1–12, 2016.

[36] W. Tan *et al.*, "Toronto-3D: A large-scale mobile LiDAR dataset for semantic segmentation of urban roadways," in *Proc. IEEE Conf. Comput. Vis. Pattern Recognit. Workshops*, 2020, pp. 797–806.

[37] B. Zhou, A. Khosla, A. Lapedriza, A. Oliva, and A. Torralba, "Learning deep features for discriminative localization," in *Proc. IEEE Conf. Comput. Vis. Pattern Recognit. (CVPR)*, Jun. 2016, pp. 2921–2929, doi:10.1109/CVPR.2016.319.

[38] M. Atzmon, H. Maron, and Y. Lipman, "Point convolutional neural networks by extension operators," *arXiv:1803.10091*, 2018. [Online]. Available: http://arxiv.org/abs/1803.10091

[39] Y. Xu, T. Fan, M. Xu, L. Zeng, and Y. Qiao, "SpiderCNN: Deep learning on point sets with parameterized convolutional filters," in *Proc. Eur. Conf. Comput. Vis.*, vol. 11212, 2018, pp. 90–105.

[40] H. Su *et al.*, "SPLATNet: Sparse lattice networks for point cloud processing," in *Proc. IEEE Conf. Comput. Vis. Pattern Recognit.*, 2018, pp. 2530–2539, doi:10.1109/CVPR.2018.00268.

[41] X. Liu, Z. Han, Y.-S. Liu, and M. Zwicker, "Point2sequence: Learning the shape representation of 3D point clouds with an attention-based sequence to sequence network," in *AAAI Conf. Artif. Intell.*, vol. 33, no. 01, 2019, pp. 8778–8785.

[42] W. Wang, R. Yu, Q. Huang, and U. Neumann, "SGPN: similarity group proposal network for 3d point cloud instance segmentation," in *Proc. IEEE Conf. Comput. Vis. Pattern Recognit.*, 2018, pp. 2569–2578.

[43] B. Graham, M. Engelcke, and L. Van Der Maaten, "3D semantic segmentation with submanifold sparse convolutional networks," in *Proc. IEEE Conf. Comput. Vis. Pattern Recognit.*, 2018, pp. 9224–9232.

[44] W. Wu, Z. Qi, and L. Fuxin, "PointConv: Deep convolutional networks on 3D point clouds," in *Proc. IEEE Conf. Comput. Vis. Pattern Recognit.*, Jun. 2019, pp. 9621–9630, doi:10.1109/CVPR.2019.00985.

[45] X. Liu, Z. Han, Y.-S. Liu, and M. Zwicker, "Point-Voxel CNN for efficient 3D deep learning," in *Adv. Neural Inf. Process. Syst.*, vol. 32, 2019, pp. 963–973.

[46] Y. Liu, B. Fan, S. Xiang, and C. Pan, "Relation-shape convolutional neural network for point cloud analysis," in *Proc. IEEE Conf. Comput. Vis. Pattern Recognit.*, 2019, pp. 8895–8904.

[47] H. Thomas *et al.*, "KPconv: Flexible and deformable convolution for point clouds," in *Proc. IEEE Int. Conf. Comput. Vis.*, 2019, pp. 6411–6420.

[48] J. Mao, X. Wang, and H. Li, "Interpolated convolutional networks for 3D point cloud understanding," in *Proc. IEEE Int. Conf. Comput. Vis.*, 2019, pp. 1578–1587.

[49] Y. Liu, B. Fan, G. Meng, J. Lu, S. Xiang, and C. Pan, "Densepoint: Learning densely contextual representation for efficient point cloud processing," in *Proc. IEEE Int. Conf. Comput. Vis.*, 2019, pp. 5239–5248.

[50] M. Xu, R. Ding, H. Zhao, and X. Qi, "PAConv: Position adaptive convolution with dynamic kernel assembling on point clouds," in *Proc. IEEE Conf. Comput. Vis. Pattern Recognit.*, 2021, pp. 3173–3182.

[51] L. Ma, Y. Li, J. Li, W. Tan, Y. Yu, and M. A. Chapman, "Multi-scale point-wise convolutional neural networks for 3D object segmentation from LiDAR point clouds in large-scale environments," *IEEE Trans. Intell. Transport. Syst.*, vol. 22, no. 2, pp. 821–836, 2019.

[52] Y. Li, L. Ma, Z. Zhong, D. Cao, and J. Li, "TGNet: Geometric graph CNN on 3-D point cloud segmentation," *IEEE Trans. Geosci. Remote Sens.*, vol. 58, no. 5, pp. 3588–3600, 2019.